Quantum Monte Carlo simulations of the two dimensional single band Hubbard model.

F.F. Assaad[†]

IPS, ETH, Zürich, Switzerland

(26. III. 1990)

Abstract

We present in detail a version of the ground state algorithm proposed by Sorella et al. and apply it to the two dimensional single band Hubbard Hamiltonian. Performing a Quantum Monte Carlo simulation based on Langevin dynamics, we study the sign problem. Our findings show that the average sign decreases exponentially with the inverse temperature. We equally study the momentum distribution and spin structure of the ground state. At half filling, we find evidence for an antiferromagnetic insulating ground state. Away from half band fillings, the antiferromagnetic state is destroyed leaving place to an incommensurate spin density wave.

[†] Also at : Institute für Theoretische Physik, ETH-Hönggerberg, Zürich.

Introduction

The study of strongly correlated fermion systems has been stimulated by the discovery of high temperature superconductors. In particular, Anderson [1] has suggested that the two dimensional Hubbard model was a good starting point for the understanding of high temperature superconductivity. In this paper, we report on Quantum Monte Carlo (Q.M.C.) simulations of the two dimensional single band Hubbard hamiltonian. At present, no exact analytical solutions are known for the above mentioned model or related models such as the t-J hamiltonian [2]. Approximate theories thus have to be tested against numerical simulations on finite size clusters. There are several ways of performing such calculations. The exact diagonalization method has been applied to the above mentioned models [3, 4] but has the major drawback of being limited to very small clusters. Calculations on

larger clusters may be carried out with Q.M.C. methods. Although appealing, the Q.M.C. method generates it's own set of problems such as, up to recently, the onset of numerical instabilities at low temperatures and the yet unsolved sign problem. There are two main ways to tackle a Q.M.C. simulation of the Hubbard model; the finite temperature, and the ground state algorithm. The finite temperature algorithm is based on the evaluation of the grand canonical partition function and produces thermodynamic quantities [5, 6]. The ground state algorithm was introduced by Sugiyama and Koonin [7] and later on improved and applied to the Hubbard model by Sorella et al. [8]. The basic idea, is to filter out the ground state wave function from a given trial wave function. Both algorithms are subject to the above mentioned problems. Following ideas proposed by Sorella et al., we present a way of circumventing the occurrence of numerical instabilities at low temperatures. The unique problem which still continues to plague Q.M.C. simulations of interacting fermion systems is the sign problem.

In the first section, we present a detailed study of the ground state algorithm. We have carried out a continuous Hubbard-Stratonovic transformation and sampled the probability distribution with Langevin dynamics. Another approach consists in carrying out a discrete Hubbard-Stratonovic transformation which leads to standard Metropolis sampling techniques [9]. The major issue concerning the algorithm is the dependence of the average sign on the temperature. Unlike Sorella et al., we find the average sign to decrease exponentially with growing inverse temperatures. Our algorithm differs from that of Sorella et al. in the fact that we have not modified the statistical weight under assumption that the average sign is bounded from below in the limit of vanishing temperatures.

In the second section we discuss our numerical results. We test the validity of the algorithm on small clusters and analyse all parameters yielding systematic errors. We then study the dependence of the average sign on the temperature, on site Coulomb repulsion, and band filling. Our results show that for certain band fillings and on site Coulomb repulsions, the exponential decay of the average sign is slow enough so as to reach high inverse temperatures without being confronted to a major sign problem. We finally present numerical data on the spin structure and momentum distribution of the Hubbard model for lattice sizes ranging from 8×8 to 10×10, on site Coulomb repulsions of $U/t = 2, \cdots, 4$ and band fillings of $\rho = 0.41, \cdots, 1$. We have compared our results to a mean field approximation. In the third section, we draw some conclusions. Preliminary results of this work were already given in ref. [10]

1   The Method - Basic Formalism

The Hubbard model we have considered is defined by:

$$H = -t \sum_{\substack{\langle i,j \rangle \\ \sigma}} (c_{i,\sigma}^\dagger c_{j,\sigma} + h.c.) + U \sum n_{i,\uparrow} n_{i,\downarrow} \tag{1}$$

where i,j denote sites on a square lattice, $c_{i,\sigma}^\dagger, c_{i,\sigma}$ create and annihilate electrons with z-component of spin σ on site i, $\langle i,j \rangle$ is a sum over next neighbors, and $n_{i,\sigma} = c_{i,\sigma}^\dagger c_{i,\sigma}$. We have adopted $t = 1$ to set the energy scale, and imposed periodic boundary conditions.

We evaluate ground state expectations values of observables through:

$$\langle O \rangle_0 = \frac{\langle \Psi_0 | O | \Psi_0 \rangle}{\langle \Psi_0 | \Psi_0 \rangle} = \lim_{\beta \to \infty} \frac{\langle \Psi_T | e^{-\beta H/2} O e^{-\beta H/2} | \Psi_T \rangle}{\langle \Psi_T | e^{-\beta H} | \Psi_T \rangle} \tag{2}$$

where $|\Psi_0\rangle$ is the ground state wave function, $|\Psi_T\rangle$ a trial wave function not orthogonal to the ground state, and β the inverse temperature (imaginary time). The imaginary time propagators on each side of the observable filter out the exited states in the trial wave function so as to yield the ground state wave function. In practice, the right hand side of equation (2) is evaluated at a finite β chosen large enough so that the thus produced errors may be included in the statistical errors. Such a choice of β depends on the trial wave function as well as on the type of observable one wishes to evaluate. We denote by $|\Psi_i\rangle$ the eigenvectors of (1) and by Δ the energy gap $E_1 - E_0$. The right hand side of equation (2) may then be written as:

$$\frac{\langle \Psi_T | e^{-\beta H/2} O e^{-\beta H/2} | \Psi_T \rangle}{\langle \Psi_T | e^{-\beta H} | \Psi_T \rangle} =$$
$$\frac{|\alpha_0|^2 \langle \Psi_0 | O | \Psi_0 \rangle + e^{-\beta \Delta/2} (\alpha_0 \alpha_1^\dagger \langle \Psi_1 | O | \Psi_0 \rangle + h.c.) + O(e^{-\beta \Delta})}{|\alpha_0|^2 \langle \Psi_0 | \Psi_0 \rangle + O(e^{-\beta \Delta})},$$
$$|\Psi_T\rangle = \sum_i \alpha_i |\Psi_i\rangle, \quad \alpha_i = \langle \Psi_i | \Psi_T \rangle \tag{3}$$

If the observable commutes with the hamiltonian, the eigenvectors $|\Psi_i\rangle$ may be chosen so as to satisfy $\langle \Psi_1 | O | \Psi_0 \rangle = 0$ so that the error is proportional $e^{-\beta \Delta}$. Observables which do not commute with the Hamiltonian have to be evaluated at larger inverse temperatures since the error is proportional to $e^{-\beta \Delta/2}$.

We will first compute the denominator of (2) and then show how observables may be evaluated. We have used a Trotter decomposition and a Hubbard-Stratonovic transformation. The aim is to write the complex time propagator as

a product of exponentials of one body operators which may be integrated. We furthermore require the trial wave function to be a Slater determinant given by:

$$|\Psi_T\rangle = \prod_{\nu,\sigma} c_{\nu,\sigma}^\dagger |0\rangle \tag{4}$$

where $c_{\nu,\sigma}^\dagger$ are electron creation operators. The Trotter decomposition we used reads :

$$
\begin{aligned}
e^{-\beta H} &= (e^{-\Delta\tau H})^L \\
&= [e^{-\Delta\tau T/2} e^{-\Delta\tau V} e^{-\Delta\tau T/2} + O(\Delta\tau^3 U^2)]^L \\
&= [e^{-\Delta\tau T/2} e^{-\Delta\tau V} e^{-\Delta\tau T/2}]^L + O[(\Delta\tau U)^2]
\end{aligned}
\tag{5}
$$

where $\beta = \Delta\tau L$ and T, V are the kinetic, potential terms of (1). The above Trotter decomposition yields a systematic error of the order of $(\Delta\tau U)^2$. Precise results are thus obtained by extrapolating to the limit $\Delta\tau \to 0, \Delta\tau L = \beta$.

The exponential of the two body operator V is reduced to the exponential of a one body operator at the cost of an auxiliary field Φ. Since we have opted for Langevin dynamics we carry out a continuous Hubbard-Stratonovic transformation which reads:

$$e^{-U\Delta\tau n_\downarrow n_\uparrow} = \int \frac{d\Phi}{\sqrt{2\pi}} e^{-\Phi^2/2 - \lambda\Phi(n_\uparrow - n_\downarrow) - \mu(n_\uparrow + n_\downarrow)} \tag{6}$$

where $\lambda = \sqrt{\Delta\tau U}$ and $\mu = \Delta\tau U/2$. Substituting (6) in (5) yields:

$$
\begin{aligned}
\langle \Psi_T | e^{-\beta H} | \Psi_T \rangle = e^{-\beta U(N^\uparrow + N^\downarrow)/2} \int [d\Phi] e^{-\sum_{i,\tau} \Phi_{i,\tau}^2/2} \\
\times \langle \Psi_T | U_\Phi^\uparrow(\beta,0) | \Psi_T \rangle \langle \Psi_T | U_\Phi^\downarrow(\beta,0) | \Psi_T \rangle
\end{aligned}
\tag{7}
$$

where τ runs from time slice 1 to L, $N^{\uparrow(\downarrow)}$ is the number of spin up (down) electrons in the trial wave function, $[d\Phi] = \prod_{i,\tau} d\Phi_{i,\tau}/\sqrt{2\pi}$ and

$$U_\Phi^\uparrow(\beta,0) = \prod_{\tau=1}^L e^{-\Delta\tau T^\uparrow/2} e^{-\lambda \sum_i \Phi_{i,\tau} n_{i,\uparrow}} e^{-\Delta\tau T^\uparrow/2}$$

$$U_\Phi^\downarrow(\beta,0) = \prod_{\tau=1}^L e^{-\Delta\tau T^\downarrow/2} e^{\lambda \sum_i \Phi_{i,\tau} n_{i,\downarrow}} e^{-\Delta\tau T^\downarrow/2}.$$

Since the propagator $U_\Phi^{\uparrow(\downarrow)}(\beta,0)$ is a product of exponentials of one body operators, the quantity $\langle \Psi_T | U_\Phi^{\uparrow(\downarrow)}(\beta,0) | \Psi_T \rangle$ may be written a determinant of an $N^{\uparrow(\downarrow)} \times N^{\uparrow(\downarrow)}$ matrix $G^{\uparrow(\downarrow)}$. Assuming for the moment that the product of the up and down spin determinants is positive definite, we may write:

$$\langle \Psi_T | e^{-\beta H} | \Psi_T \rangle = e^{-\beta U(N^\uparrow + N^\downarrow)/2} \int [d\Phi] e^{-S_{eff}(\Phi)} \tag{8}$$

where

$$S_{eff}(\Phi) \; = \; \sum_{i,\tau} \Phi_{i,\tau}^2/2 - \ln[\det(G^\uparrow(\Phi,\beta))\det(G^\downarrow(\Phi,\beta))],$$

$$G_{\mu,\nu}^{\uparrow(\downarrow)}(\Phi,\beta) \; = \; \langle 0|c_{\mu,\uparrow(\downarrow)} U_\Phi^{\uparrow(\downarrow)}(\beta,0) c_{\nu,\uparrow(\downarrow)}^\dagger|0\rangle.$$

We evaluate the above matrix elements by introducing a complete set of vectors $|i\rangle \equiv c_i^\dagger|0\rangle$ between each time slice.

$$G_{\mu,\nu}(\Phi,\beta) \; = \; \sum_{i_1\cdots i_L} e^{\pm\lambda(\Phi_{i_1,1}+\cdots+\Phi_{i_L,L})} \tag{9}$$

$$\times \;\; \langle\mu|e^{-\Delta\tau T/2}|i_1\rangle\langle i_1|e^{-\Delta\tau T}|i_2\rangle\cdots\langle i_{L-1}|e^{-\Delta\tau T}|i_L\rangle\langle i_L|e^{-\Delta\tau T/2}|\nu\rangle.$$

(Note: we have omitted the spin indices.) The minus (plus) sign refers to spin up (down) matrix elements.

Using the above formalism, observables $O = O^\uparrow O^\downarrow$ may be evaluated through:

$$\langle O\rangle_0 = \frac{\int[d\Phi]e^{-S_{eff}(\Phi)}\langle\langle O^\uparrow\rangle\rangle(\Phi)\langle\langle O^\downarrow\rangle\rangle(\Phi)}{\int d[\Phi]e^{-S_{eff}(\Phi)}} \tag{10}$$

where

$$\langle\langle O^{\uparrow(\downarrow)}\rangle\rangle(\Phi) = \frac{\langle\Psi_T|U_\Phi^{\uparrow(\downarrow)}(\beta,\beta/2)O^{\uparrow(\downarrow)}U_\Phi^{\uparrow(\downarrow)}(\beta/2,0)|\Psi_T\rangle}{\langle\Psi_T|U_\Phi^{\uparrow(\downarrow)}(\beta,0)|\Psi_T\rangle}.$$

For observables of the form

$$O = \sum_{i,j} c_i^\dagger A_{i,j} c_j,$$

one has (we omit the spin indices):

$$\langle\langle O\rangle\rangle(\Phi) = \text{Tr}\{G^{-1}(\Phi,\beta)\hat{O}(\Phi,\beta)\} \qquad \text{where}$$

$$\hat{O}_{\mu,\nu}(\Phi,\beta) = \sum_{i,j}\langle\mu|U_\Phi(\beta,\beta/2)|i\rangle A_{i,j}\langle j|U_\Phi(\beta/2,0)|\nu\rangle. \tag{11}$$

Observables of the form

$$O = (\sum_{i,j} c_i^\dagger A_{i,j}^{(1)} c_j)(\sum_{i',j'} c_{i'}^\dagger A_{i',j'}^{(2)} c_{j'})$$

yield

$$\langle\langle O\rangle\rangle(\Phi) = \langle\langle O^{(1)}\rangle\rangle(\Phi)\langle\langle O^{(2)}\rangle\rangle(\Phi) - \tag{12}$$

$$- \text{Tr}\{G^{-1}(\Phi,\beta)\hat{O}^{(1)}(\Phi,\beta)G^{-1}(\Phi,\beta)\hat{O}^{(2)}(\Phi,\beta)\} + \text{Tr}\{G^{-1}(\Phi,\beta)\hat{\hat{O}}(\Phi,\beta)\}$$

where

$$\hat{\hat{O}}_{\mu,\nu}(\Phi,\beta) = \sum_{i,j,i'}\langle\mu|U_\Phi(\beta,\beta/2)|i\rangle A_{i,i'}^{(1)} A_{i',j}^{(2)}\langle j|U_\Phi(\beta/2,0)|\nu\rangle.$$

Note that for $O = c_p^\dagger c_q c_r^\dagger c_s$ equation (12) reduces to Wick's theorem:

$$\langle\langle c_p^\dagger c_q c_r^\dagger c_s\rangle\rangle(\Phi) = \langle\langle c_p^\dagger c_q\rangle\rangle(\Phi)\langle\langle c_r^\dagger c_s\rangle\rangle(\Phi) + \langle\langle c_p^\dagger c_s\rangle\rangle(\Phi)\langle\langle c_q c_r^\dagger\rangle\rangle(\Phi). \tag{13}$$

Observables which do not commute with the hamiltonian (1), have somewhat worse statistics than observables which commute with the Hamiltonian since in the latter case the quantity $\langle\langle O\rangle\rangle(\Phi)$ may be evaluated on each time slice.

As mentioned above, the sampling of the probability distribution $e^{-S_{eff}(\Phi)}$ was carried out with second order discretized Langevin dynamics [11, 12]. We consider the Hubbard-Stratonovic variables $\Phi_{i,\tau}$ to be time dependent. Their time evolution is given by the Langevin equation:

$$\Phi_{i,\tau}(t + \delta t) = \Phi_{i,\tau}(t) - \tag{14}$$
$$\frac{\delta t}{2}\left(\left.\frac{\partial S_{eff}(\Phi)}{\partial \Phi_{i,\tau}}\right|_{\Phi_{i,\tau}=\Phi_{i,\tau}(t)} + \left.\frac{\partial S_{eff}(\Phi)}{\partial \Phi_{i,\tau}}\right|_{\Phi_{i,\tau}=\Phi_{i,\tau}^{(1)}(t+\delta t)}\right) + \sqrt{2\delta t}\,\eta_{i,\tau}(t).$$

Here, $\eta_{i,\tau}(t)$ are Gaussian distributed random variables:

$$\langle\eta_{i,\tau}(t)\rangle = 0$$
$$\langle\eta_{i,\tau}(t)\eta_{i',\tau'}(t')\rangle = \delta_{\tau,\tau'}\delta_{t,t'}\delta_{i,i'}$$

and

$$\Phi_{i,\tau}^{(1)}(t + \delta t) = \Phi_{i,\tau}(t) - \delta t\left.\frac{\partial S_{eff}(\Phi)}{\partial \Phi_{i,\tau}}\right|_{\Phi_{i,\tau}=\Phi_{i,\tau}(t)} + \sqrt{2\delta t}\,\eta_{i,\tau}(t).$$

Note that the same Gaussian variables are used for calculating $\Phi_{i,\tau}^{(1)}(t + \delta t)$ and $\Phi_{i,\tau}(t + \delta t)$. The error produced by the above discretization of the Langevin equation is of order δt^2. In the limit of very small time steps, the random noise (of order $\sqrt{\delta t}$) greatly dominates the drift term (of order δt). The drift term in (14) is calculated using:

$$\frac{\partial S_{eff}(\Phi)}{\partial \Phi_{i,\tau}} = \Phi_{i,\tau} - \sum_{\sigma=\uparrow,\downarrow}\text{Tr}\left\{(G^\sigma)^{-1}\frac{\partial G^\sigma}{\partial \Phi_{i,\tau}}\right\} \quad \text{where} \tag{15}$$

$$\frac{\partial G_{\mu,\nu}^\sigma}{\partial \Phi_{i,\tau}} = \pm\lambda\langle\mu|U_\Phi^\sigma(\beta,\beta_\tau)|i\rangle\langle i|U_\Phi^\sigma(\beta_\tau,0)|\nu\rangle\,,\ \beta_\tau = \tau\cdot\Delta\tau.$$

The $+ (-)$ sign refers to down (up) spin. Observables are measured using:

$$\langle O\rangle_0 = \lim_{M\to\infty}\frac{1}{M}\sum_{m=1}^{M}\langle\langle O\rangle\rangle(\Phi(m\delta t)). \tag{16}$$

In practice, a finite number of Langevin iterations are carried out. The thus produced uncertainty, $\sigma(O)$, may be estimated by:

$$\sigma(O) = \frac{1}{\sqrt{N}} \sqrt{\frac{1}{M} \sum_{m=1}^{M} \langle\langle O \rangle\rangle^2 (\Phi(m\delta t)) - \langle O \rangle_0^2}. \qquad (17)$$

Here, N is the number of independent values of $\langle\langle O \rangle\rangle(\Phi)$ along the Langevin walk. More information on the estimation of the uncertainty is given in [13, 14].

1.1 Numerical instabilities and sign problem

On finite precision machines, an accurate evaluation of the matrix elements $G_{\mu,\nu}(\Phi, \beta)$ (10) becomes increasingly difficult as the inverse temperature is enhanced. We illustrate this by considering the special case $U = 0$. The eigenvalues of $U_\Phi(\beta, 0)$ are then equal to $e^{-\beta\epsilon(\vec{k})}$ where $\epsilon(\vec{k})$ denotes the single particle eigenvalues of the kinetic energy. For the two dimensional Hubbard model on a square lattice, the eigenvalues of $U_\Phi(\beta, 0)$ range from $e^{-\beta 4t}$ to $e^{\beta 4t}$. In a straightforward calculation of $G_{\mu,\nu}(\Phi, \beta)$ contributions from small eigenvalues of $U_\Phi(\beta, 0)$ will be lost in round off errors when β gets big. In order to circumvent this problem, a set of matrix decomposition methods were introduced by several authors [8, 6]. Consider the set of vectors $U_\Phi(\beta, 0)|\nu\rangle$, $\nu = 1 \cdots N^{\uparrow(\downarrow)}$. At large β they will all collapse into the subspace spanned by the set of eigenvectors of $U_\Phi(\beta, 0)$ with the largest eigenvalues. In order to circumvent this, we split the imaginary time propagation into n imaginary time intervals $\Delta\beta$. After each propagation over $\Delta\beta$, we orthonormalize the set of vectors $U_\Phi(\Delta\beta, 0)|\nu\rangle$. The matrix elements (10) are now calculated using:

$$\tilde{G}_{\mu,\nu}(\Phi, \beta) = \sum_{\substack{\mu_1 \cdots \mu_{n-m} \\ \nu_1 \cdots \nu_m}} \qquad (18)$$

$$\langle \mu_1 | U_\Phi(\beta, \beta - \Delta\beta) \, (\mathrm{TD})^{\mathrm{L},1}_{\mu_1,\mu_2} U_\Phi(\beta - \Delta\beta, \beta - 2\Delta\beta) \, (\mathrm{TD})^{\mathrm{L},2}_{\mu_2,\mu_3} \cdots$$

$$U_\Phi((m+1)\Delta\beta, m\Delta\beta) \, (\mathrm{TD})^{\mathrm{L},n-m}_{\mu_{n-m},\mu} U_\Phi(m\Delta\beta, (m-1)\Delta\beta) \, (\mathrm{DT})^{\mathrm{R},m}_{\nu,\nu_m} \cdots$$

$$(\mathrm{DT})^{\mathrm{R},2}_{\nu_3,\nu_2} U_\Phi(2\Delta\beta, \Delta\beta) \, (\mathrm{DT})^{\mathrm{R},1}_{\nu_2,\nu_1} U_\Phi(\Delta\beta, 0)|\nu_1\rangle$$

Here, D is a diagonal $N^{\uparrow(\downarrow)} \times N^{\uparrow(\downarrow)}$ matrix and T a triangular matrix of same dimension. T carries out a Gram-Schmidt orthogonalization, and D normalizes

the vectors. For small values of $\Delta\beta$ (we typically used $\Delta\beta = 10\Delta\tau$), the round of errors in $\tilde{G}_{\mu,\nu}(\Phi, \beta)$ are negligible. Furthermore, the matrix $\tilde{G}_{\mu,\nu}(\Phi, \beta)$ is well conditioned.

Clearly, the above stabilization of the algorithm makes sense only if the physical quantities and the Langevin dynamic remain invariant. We define the partial derivative of $\tilde{G}_{\mu,\nu}(\Phi, \beta)$ with respect to $\Phi_{i,\tau}$ where β_τ ($\equiv \tau \cdot \Delta\tau$) is included in the interval $[m\Delta\beta, (m-1)\Delta\beta]$ by:

$$\frac{\partial \tilde{G}_{\mu,\nu}(\Phi, \beta)}{\partial \Phi_{i,\tau}} \equiv \pm\lambda \sum_{\mu',\nu'} \mathcal{L}^m_{\mu,\mu'} \langle \mu' | U_\Phi(\beta, \beta_\tau) | i \rangle \langle i | U_\Phi(\beta_\tau, 0) | \nu' \rangle \mathcal{R}^m_{\nu',\nu} = \qquad (19)$$

$$\left(\mathcal{L}^m \frac{\partial G(\Phi, \beta)}{\partial \Phi_{i,\tau}} \mathcal{R}^m \right)_{\mu,\nu}.$$

Here we have defined:

$$\mathcal{L}^m \equiv \left((\mathrm{TD})^{\mathrm{L},1} \cdots (\mathrm{TD})^{\mathrm{L},n-m} \right)^{\mathrm{T}} \quad \text{and}$$

$$\mathcal{R}^m \equiv \left((\mathrm{DT})^{\mathrm{R},m} \cdots (\mathrm{DT})^{\mathrm{R},1} \right)^{\mathrm{T}}.$$

Since $\tilde{G} = \mathcal{L}^m G \mathcal{R}^m$ and due to the cyclic properties of the trace, the drift term in the Langevin equation (15) is invariant under the substitution $G \to \tilde{G}$. In the same way, one can show that the stabilization leaves the quantities $\langle\langle O \rangle\rangle(\Phi)$ (11) invariant.

Up till now, we have assumed that the product of the determinants (8) was positive for all values of the Hubbard-Stratonovic fields. This assumption is unfortunately not always satisfied. In the latter case, the effective action $S_{eff}(\Phi)$ (8) is replaced by:

$$\tilde{S}_{eff}(\Phi) = \sum_{i,\tau} \Phi_{i,\tau}^2 / 2 - \ln | \det(G^\uparrow(\Phi, \beta)) \det(G^\downarrow(\Phi, \beta)) |, \qquad (20)$$

and the sampling is done with respect to the probability distribution $e^{-\tilde{S}_{eff}(\Phi)}$. Observables are then estimated using:

$$\langle O \rangle_0 = \frac{\int [d\phi] e^{-\tilde{S}_{eff}(\Phi)} \mathrm{sign}(\Phi) \langle\langle O \rangle\rangle(\Phi)}{\int [d\phi] e^{-\tilde{S}_{eff}(\Phi)} \mathrm{sign}(\Phi)} \simeq \frac{O^+ - O^-}{Z^+ - Z^-}. \qquad (21)$$

Here,

$$Z^\pm = \sum_{m=1}^M \delta_{\pm 1, \mathrm{sign}(\Phi(m\delta t))}$$

$$O^\pm = \sum_{m=1}^M \delta_{\pm 1, \mathrm{sign}(\Phi(m\delta t))} \langle\langle O \rangle\rangle(\Phi(m\delta t))),$$

and sign(Φ) denotes the sign of the product of the two determinants. When the number of sampled positive configurations is comparable to the number of negative ones, the uncertainty on $\langle O \rangle_0$ becomes very big due to the uncertainty on $Z^+ - Z^-$. Since the uncertainty scales as the inverse square root of the computer time, simulations become extremely expensive when the average sign $(Z^+ - Z^-)/(Z^+ + Z^-)$ is small. A reduction of the fluctuation of the average sign may be achieved by carrying out simultaneously two correlated Langevin simulations [15].

Fortunately, in the half filled band case, particle hole symmetry protects us from a sign problem provided we choose an appropriate trial wave function. Choosing $|\Psi_T\rangle$ to be a Fermi sea at half filling,

$$|\Psi_T\rangle = \prod_{\substack{\vec{k},\sigma \\ \epsilon(\vec{k}) < \epsilon_{Fermi}}} c^{\dagger}_{\vec{k},\sigma} |0\rangle, \tag{22}$$

and applying the transformation [16]

$$h^{\dagger}_i = (-1)^i c_i, \qquad h_i = (-1)^i c^{\dagger}_i \tag{23}$$

on $G^{\downarrow}(\Phi, \beta)$ yields

$$\det(G^{\downarrow}(\Phi, \beta)) = e^{\lambda \sum_{i,\tau} \Phi_{i,\tau}} \det(G^{\uparrow}(\Phi, \beta)) \tag{24}$$

so that no sign problem occurs. Other trial wave functions such as the antiferromagnetic state

$$|\Psi_T\rangle = \prod_{\substack{i \\ (-1)^i = 1}} c^{\dagger}_{i,\uparrow} \prod_{\substack{i \\ (-1)^i = -1}} c^{\dagger}_{i,\downarrow} |0\rangle \tag{25}$$

equally yield no sign problem. In the non half filled band case there seems to be no symmetry which protects us from the sign problem.

In the half filled band case, the sign of the individual determinants may change simultaneously thus producing infinite barriers in the effective action (20). Since the Langevin walk is capable of jumping over those barriers, ergodicity is satisfied (see later and [17]). However, when it lands in the proximity of a barrier, the drift term in the Langevin equation (14) may become extremely large and destabilize the simulation. When such a situation occurs, we go back to the previous configuration of Hubbard-Stratonovic fields and carry out the integration with a smaller time step but with the same set of random numbers. The variation of the time step is taken into account when computing averages. In the non half filled band case the same method is applied to stabilize the Langevin walk. The problem of infinite barriers in the effective action may also be circumvented by performing a complex Hubbard-Stratonovic transformation which makes them finite [18].

2   Numerical results.

We present numerical results for lattice sizes ranging from 4×4 to 10×10 and at different band fillings. In the first section, we analyse all parameters yielding systematic errors; in the second the sign problem and in the third, the spin structure and momentum distribution of the two dimensional Hubbard model. Unless stated otherwise, the simulations were carried out the paramagnetic trial wave function (22).

2.1   Sources of systematic errors.

The above described method contains three parameters which produce systematic errors: the inverse temperature β, the imaginary time step $\Delta\tau$ and the Langevin time step δt. We have analysed their effect on the ground state energy per site:

$$E_0 = -\frac{t}{N_{sites}} \sum_{\substack{\langle i,j \rangle \\ \sigma}} \langle c_{i,\sigma}^\dagger c_{j,\sigma} + h.c. \rangle_0 + \frac{U}{N_{sites}} \sum_i \langle n_{i,\uparrow} n_{i,\downarrow} \rangle_0. \quad (26)$$

We have chosen a paramagnetic trial wave function (22) and $U = 4$. Figure 1 plots the expectation value of the ground state energy as a function of the inverse temperature β. Values of β greater than 10 are required to stabilize it. The same qualitative results were obtained with an antiferromagnetic trial wave function (25). The kinetic and potential energy were found to converge for values of β greater than 15.

As expected, the error produced by the second order discretized Langevin equation scales as δt^2 (figure 2). We have fitted our data to the form

$$E_0(\delta t, \beta = 13.75, \Delta\tau = 0.125) = E_0(\delta t = 0, \beta = 13.75, \Delta\tau = 0.125) + b_{\delta t}\delta t^2 \quad (27)$$

The coefficient $b_{\delta t}$ for a 4×4 lattice was found to be comparable to that of a 6×6 lattice. (4×4 : $b_{\delta t} = 3.2 \pm 0.5$, 6×6 : $b_{\delta t} = 2.8 \pm 0.4$). The number of hoppings over the infinite barriers in the effective action per Langevin time unit is shown in figure 3. Following an argument proposed by White and Wilkins [17], this quantity should scale as $\sqrt{\delta t}$. Unfortunately, our error bars are too big to justify such a fit.

Finally, the $\Delta\tau$ dependency of the ground state energy is shown in figure 4. The simulations were carried out with values of β and $\Delta\tau$ respectively large and small enough so as to neglect the systematic errors they produce. We fitted our data to the form

$$E_0(\Delta\tau, \beta = 13.75, \delta t = 0.01) = E_0(\Delta\tau = 0, \beta = 13.75, \delta t = 0.01) + b_{\Delta\tau}\Delta\tau^2. \quad (28)$$
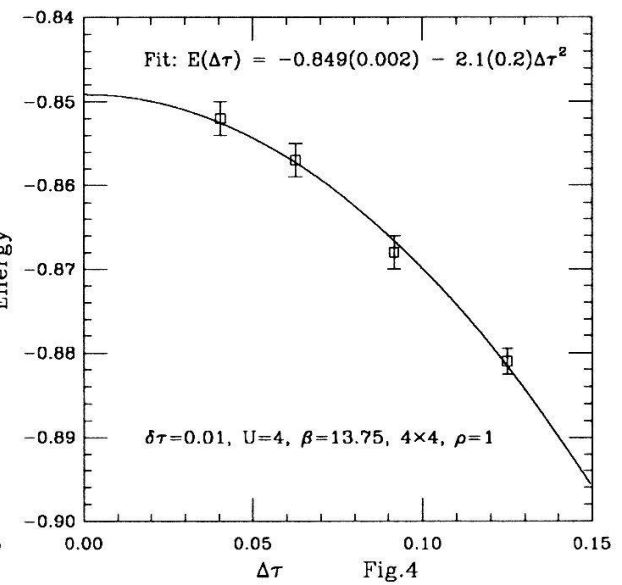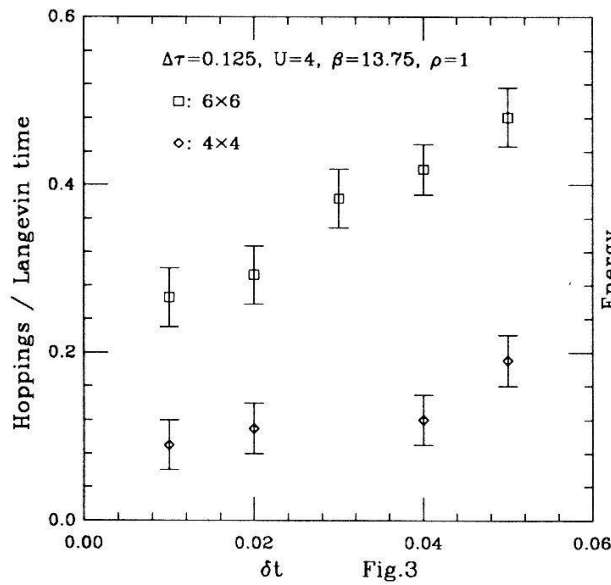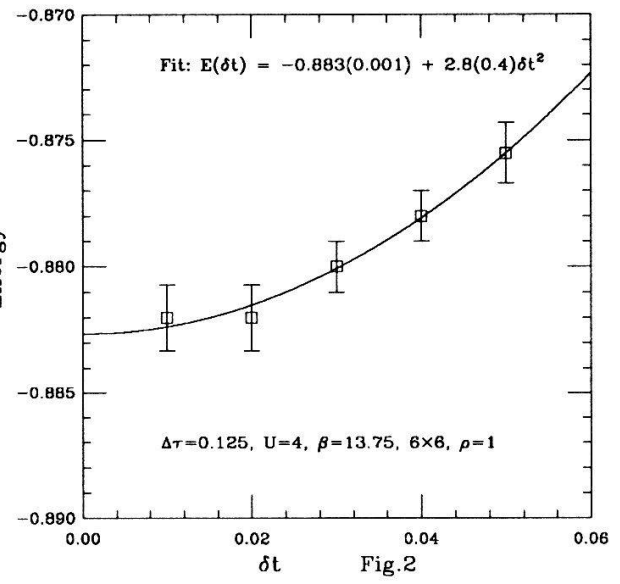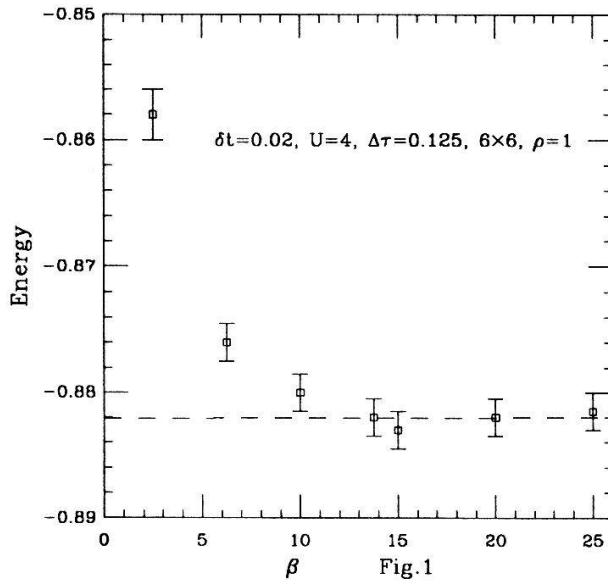
Fig.1 Ground state energy as a function of the inverse temperature for a 6 × 6 lattice at $\rho = 1$ and $U = 4$.

Fig.2 Ground state energy as a function of the Langevin time step δt for a 6 × 6 lattice at $\rho = 1$, $U = 4$ and $\beta = 13.75$.

Fig.3 Number of hoppings over infinite barriers in the effective action per unit Langevin time for 6 × 6, 4 × 4 lattices at $\rho = 1$, $U = 4$ and $\beta = 13.75$.

Fig.4 Ground state energy as a function of the imaginary time step $\Delta\tau$ for a 4 × 4 at $\rho = 1$, $U = 4$ and $\beta = 13.75$

We obtained for the 4×4 lattice $E_0(\Delta \tau = 0, \beta = 13.75, \delta t = 0.01) = -0.849 \pm 0.002$, and for the 6×6 lattice $E_0(\Delta \tau = 0, \beta = 13.75, \delta t = 0.01) = -0.852 \pm 0.002$. Again, the coefficient $b_{\Delta \tau}$ was found to be comparable for the 4×4 ($b_{\Delta \tau} = -2.1 \pm 0.2$) and 6×6 ($b_{\Delta \tau} = -1.9 \pm 0.2$) lattices. Exact diagonalization yields a ground state energy per site of $E_0 = -0.851$ for the 4×4 lattice at $U = 4$.

2.2 Sign problem.

As mentioned previously, the quantity $\det(G^{\uparrow}(\Phi, \beta)) \det(G^{\downarrow}(\Phi, \beta))$ is not positive for all values of the Hubbard-Stratonovic configurations at of half band fillings. A study of some aspects of the average sign has already been performed by Loh et al. [19]. In order to get some insight into the sign of $\det(G^{\uparrow(\downarrow)}(\Phi, \beta))$, we write the determinant as:

$$\det(G^{\uparrow(\downarrow)}(\Phi, \beta)) = \sum_{\Psi_1, \Psi_2} \langle \Psi_T | \Psi_1 \rangle \langle \Psi_2 | \Psi_T \rangle \langle \Psi_1 | U_\Phi^{\uparrow(\downarrow)}(\beta, 0) | \Psi_2 \rangle. \qquad (29)$$

Here, the sum runs over a complete set of vectors of the $N^{\uparrow(\downarrow)}$ particle vector space. We furthermore require the the states $|\Psi_{1,2}\rangle$ to be eigenvectors of the local particle number operator $n_i = c_i^\dagger c_i$. The quantity $\langle \Psi_1 | U_\Phi^{\uparrow(\downarrow)}(\beta, 0) | \Psi_2 \rangle$ is then nothing less than the sum over all world line configurations [16] propagating from the state $|\Psi_2\rangle$ to the state $|\Psi_1\rangle$. It is known, that a world line configuration has a negative weight whenever world lines wind around each other an odd number of times [21]. The magnitude of the weight of a world line configuration depends on the values of the Hubbrard-Stratonovic variables. After a sufficiently large imaginary time propagation, a world line configuration looses memory of it's initial state. The probability of having an odd number of windings per imaginary time interval thus approaches a constant P. We denote by $P(\beta)$ the probability of having a world line configuration with an odd number of windings at imaginary time β. From the above follows:

$$S(\beta) \equiv 1 - 2P(\beta) \equiv \frac{N_+(\beta) - N_-(\beta)}{N_+(\beta) + N_-(\beta)} \sim (1 - 2P)^\beta. \qquad (30)$$

Here $N_\pm(\beta)$ denotes the number of world line configurations with positive (negative) weights at imaginary time β. The quantity $S(\beta)$ decays exponentially with the inverse temperature so that in the limit of large imaginary times the number of world line configurations with positive weights is comparable to the number of world line configurations with negative weights. The sign of $\langle \Psi_1 | U_\Phi^{\uparrow(\downarrow)}(\beta, 0) | \Psi_2 \rangle$ depends on whether or not the Hubbard-Stratonovic variables render the total weight
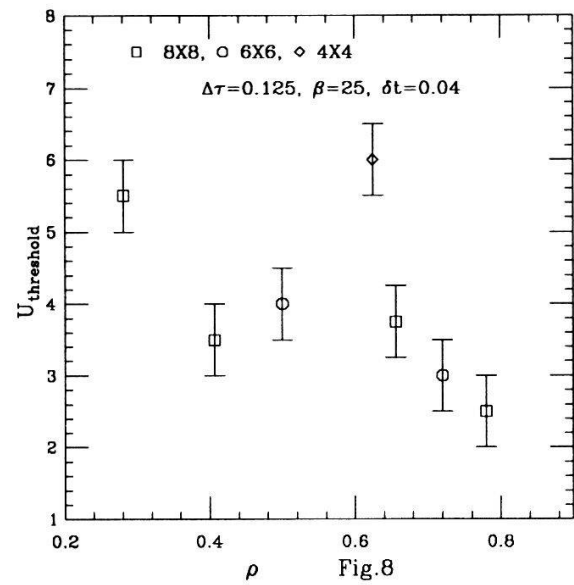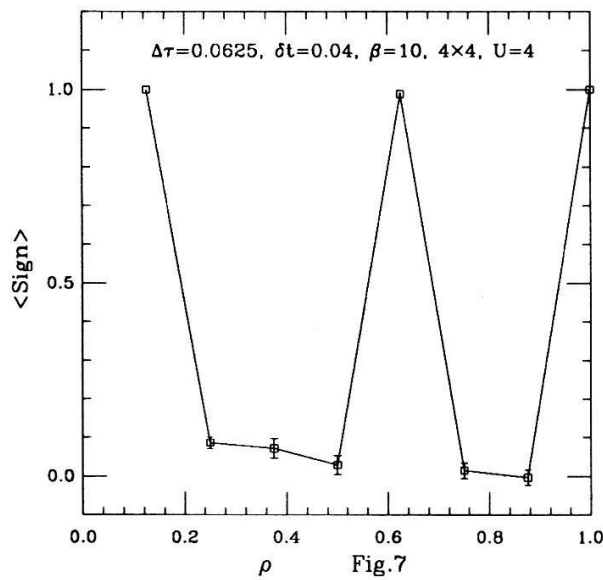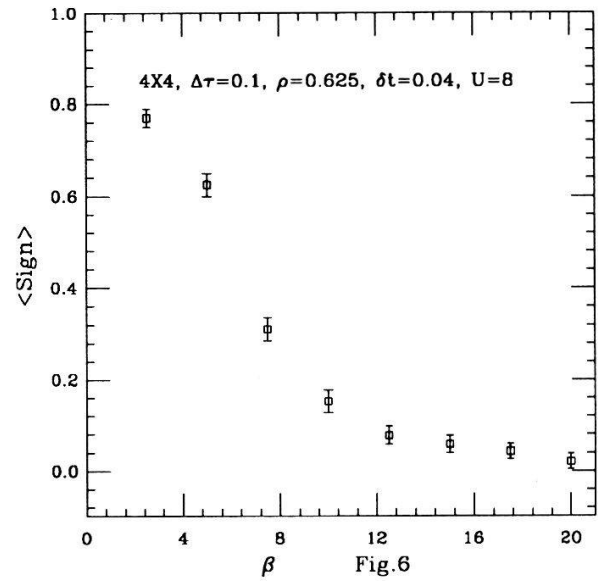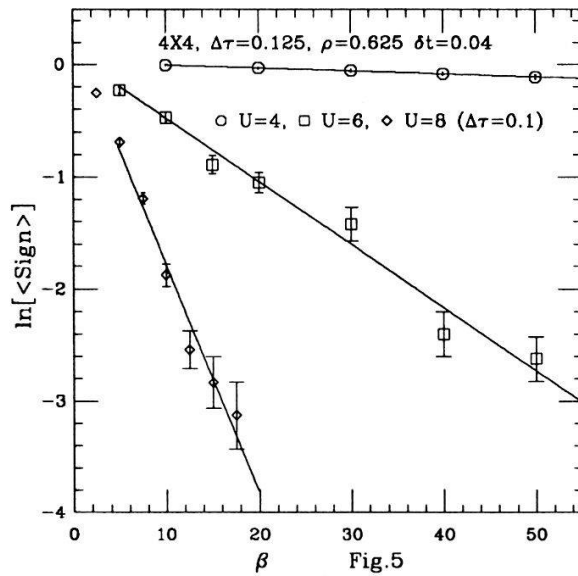
Fig.5 ln⟨sign⟩ as a function of the inverse temperature for a 4 × 4 lattice at $\rho = 0.625$, $U = 4$, $U = 6$, and $U = 8$.

**Fig.6** Average sign as a function of the inverse temperature for a 4 × 4 lattice at $\rho = 0.625$ and $U = 4$.

**Fig.7** Average sign as a function of the filling for a 4 × 4 lattice at $U = 4$ and $\beta = 10$.

Fig.8 $U_{threshold}$ as a function of the band filling at $\beta = 25$.

of the positive world line configurations, $W_+(\Phi)$, greater than that of the negative world line configurations, $W_-(\Phi)$. Since the Hubbard-Sratonovic fields undergo large fluctuations, we expect the probability that $W_-(\Phi)$ dominates $W_+(\Phi)$ to be proportional to $N_-(\beta)/(N_+(\beta) + N_-(\beta))$. The average sign of $\det(G^{\uparrow(1)}(\Phi, \beta))$ is thus expected to decay exponentially with the inverse temperature. If there is no symmetry which guarantees that $\det(G^{\uparrow}(\Phi, \beta))$ has the same sign as $\det(G^{\downarrow}(\Phi, \beta))$ for all Hubbard-Stratonovic configurations, we equally expect the average sign of $\det(G^{\uparrow}(\Phi, \beta)) \det(G^{\downarrow}(\Phi, \beta))$ to decrease exponentially with the inverse temperature. In the same way, one may argue that the average sign decreases exponentially with the lattice size.

When the on site Coulomb repulsion U is set to zero, the weight of a world line configuration is independent of the Hubbard-Stratonovic variables. As U is increased, the inhomogeneities in the Hubbard-Stratonovic variables are emphasized so that the sign of $\det(G^{\uparrow}(\Phi, \beta)) \det(G^{\downarrow}(\Phi, \beta))$ becomes increasingly sensitive to fluctuations of the Hubbard-Stratonovic variables. Figures 5 and 6 plot the average sign as a function of the inverse temperature for different values of the on site Coulomb repulsion, a 4×4 lattice and a filling of $\rho = 0.625$. Our error bars are consistent with an exponential decay of the average sign. Furthermore, the average sign decreases as the on site Coulomb repulsion U is enhanced. The here presented results are consistent with those of Loh et al. [19].

The average sign is equally strongly dependent on the band filling. Figure 7 shows the average sign as a function of the filling for a 4×4 lattice, $U = 4$ and $\beta = 10$. The fillings where the average sign is approximately 1, correspond to band fillings where the ground state of the kinetic energy is non degenerate (that is $\rho = 10/16$ and $\rho = 2/16$ for the 4×4 lattice). At such fillings, for small to moderate values of the on site Coulomb repulsion and for inverse temperatures up to $\beta = 50$, the signs of the individual determinants are nearly exclusively positive for all sampled values of the Hubbard-Stratonovic variables. In order to get some insight into this situation, we formulate $\det(G^{\uparrow}(\Phi, \beta))$ as the sum over all world lines if k (fourier) space. (i.e. the imaginary time propagation is done in k space.) The sign of a world line configuration now depends on the Hubbard-Stratonovic variables. At $U = 0$, only one world line configuration, C_0 is allowed, namely that where all world lines move along the imaginary time axis. For small to moderate values of U, the dominant world line configurations consists of small perturbations around C_0. When the filling is chosen such that $|\Psi_T\rangle$ is non degenerate with respect to the kinetic energy, all perturbations around the world line configuration C_0 involve the occupation of exited single particle eigenstates of the kinetic energy. This isn't the case when $|\Psi_T\rangle$ is degenerate. Since world line configurations with
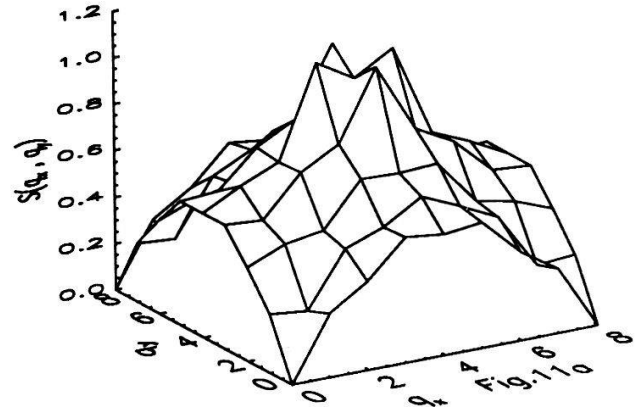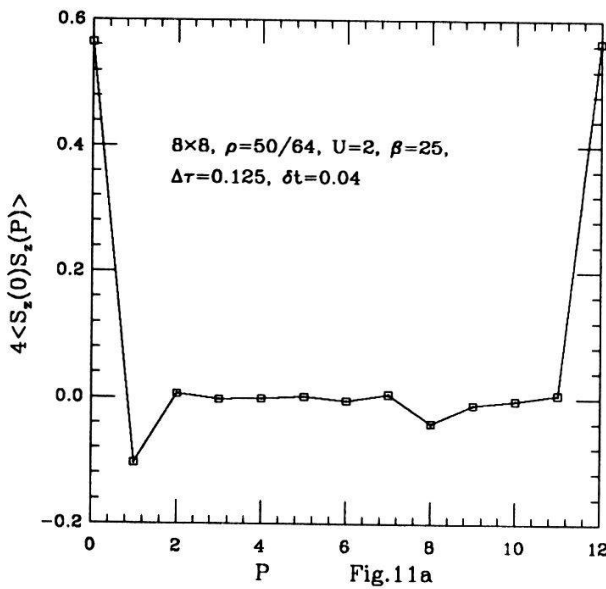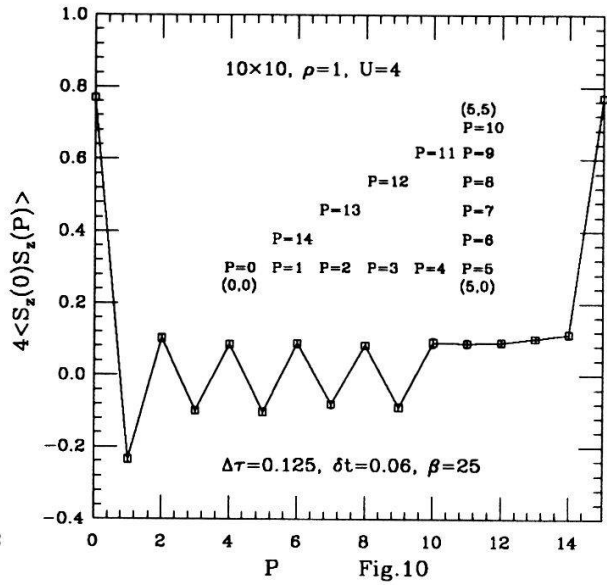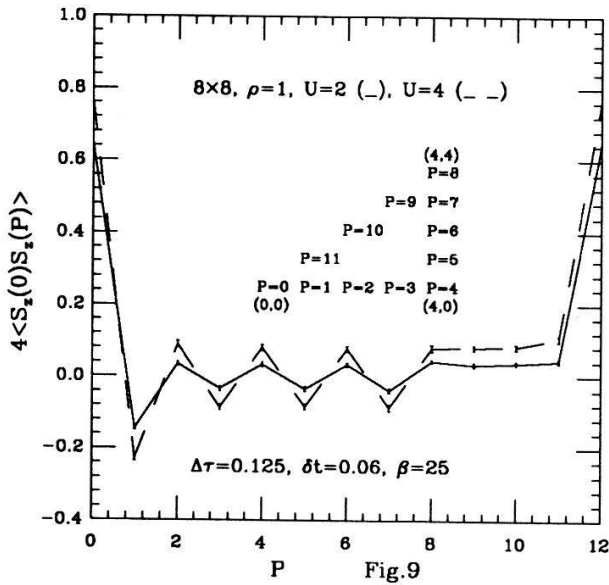
Fig.9 Spin-spin correlation function for a 8×8 lattice at $\rho = 1$, $\beta = 25$, $U = 2$ and $U = 4$. The numbering denotes the path on the two dimensional lattice: starting at $(0,0)$, going along the x-axis, then along the y-axis and diagonally back.

Fig. 10 Spin-spin correlation function for a 10×10 lattice at $\rho = 1$, $\beta = 25$ and $U = 4$.

Fig.11 Spin-spin correlation function and structure factor for a 8×8 lattice at

a) $\rho = 50/64$, $\beta = 25$ and $U = 2$. ($E_0 = -1.325 \pm 0.002$, $\langle sign \rangle = 0.94 \pm 0.03$)

negative weights are included in the set of perturbations of C_0, we expect the ratio of total positive weights to total negative weights of a world line configuration to be greater when $|\Psi_T\rangle$ is not degenerate than to that when $|\Psi_T\rangle$ is degenerate. This qualitatively explains the behavior of the average sign with respect to the filling.

As mentioned previously, simulations get extremely expensive when the average sign is small. For $\beta = 25$, figure 8 plots the maximal value of U, $U_{\text{threshold}}$, as function of the filling below which one may omit the sign problem (i.e. average sign greater than 0.7). Note that the considered fillings correspond to fillings where the trial wave function is non degenerate with respect to the kinetic energy. The results we now present were all carried out at values of U and ρ at which the sign problem was negligible.

2.3   Spin structure and momentum distribution

Confirming results from other authors, [5, 6, 8, 9, 20] we find the ground state to exhibit *long range* antiferromagnetic order at half filling and for all considered values of the on site Coulomb repulsion. Antiferromagnetic order may be detected through spin-spin correlation functions:

$$4\langle S_z(\vec{0})S_z(\vec{P})\rangle = \frac{1}{N_{sites}} \sum_{\vec{i}} \langle (n_{\vec{i},\uparrow} - n_{\vec{i},\downarrow})(n_{\vec{i}+\vec{P},\uparrow} - n_{\vec{i}+\vec{P},\downarrow})\rangle_0. \tag{31}$$

Figures 9 and 10 plot the above spin-spin correlations for $U = 2$, $U = 4$ and lattice sizes of 8×8, 10×10. The magnitude of the spin-spin correlations are comparable for both lattice sizes. In order to determine whether the ground state truly exhibits long range antiferromagnetic order simulations at larger lattice sizes are required along with a finite size scaling analysis [23]. The squared magnetization per site, $m_2 \equiv 4\langle S_z(\vec{0})S_z(\vec{0})\rangle$, is related to the double occupancy of sites through:

$$m_2 = 1 - \frac{2}{N_{sites}} \sum_{\vec{i}} \langle n_{\vec{i},\uparrow} n_{\vec{i},\downarrow}\rangle_0. \tag{32}$$

Since the double occupancy of sites involves an energy gap set by U it is expected to decrease as U is enhanced and ultimately vanish as $t/U \to 0$ where the Hubbard model reduces to the Heisenberg model. This may be seen by comparing the values of m_2 for $U = 2$ and $U = 4$.

In contrast, the *long range* antiferromagnetic order disappears when one leaves half filling. Figures 11a to 11c show spin-spin correlations as well as the magnetic
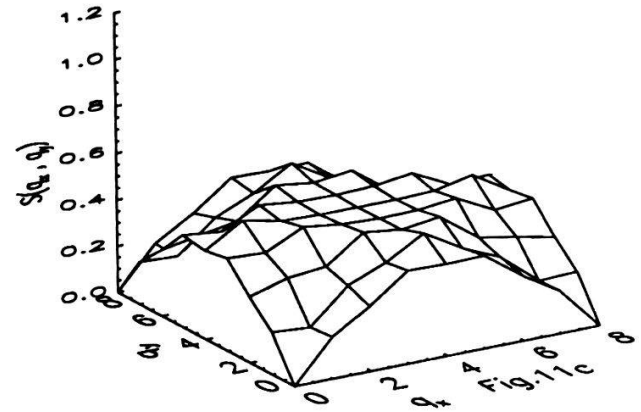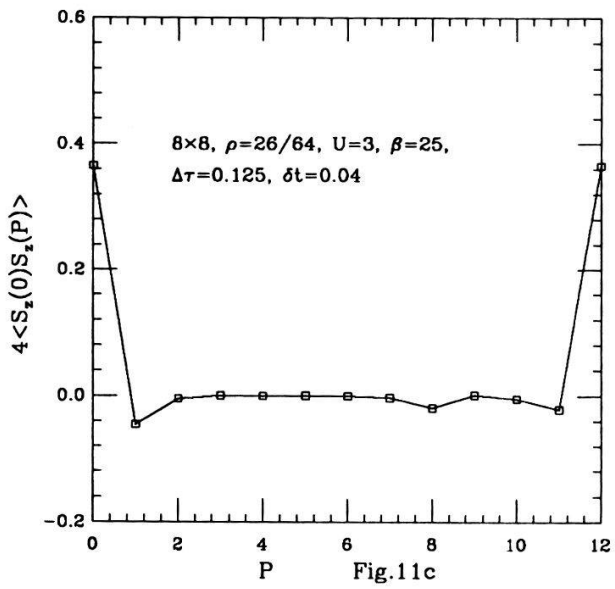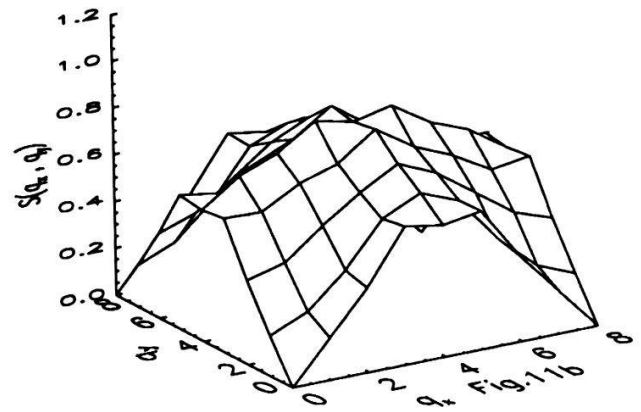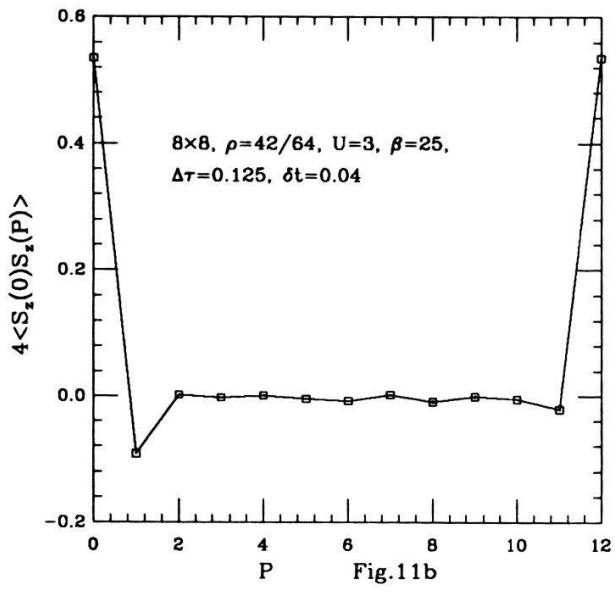
Fig.11 Spin-spin correlation function and structure factor for a 8×8 lattice at

b) $\rho = 42/64$, $\beta = 25$ and $U = 3$. ($E_0 = -1.268 \pm 0.002$, $\langle \mathrm{sign} \rangle = 0.90 \pm 0.03$)

c) $\rho = 26/64$, $\beta = 25$ and $U = 3$. ($E_0 = -1.069 \pm 0.002$, $\langle \mathrm{sign} \rangle = 0.76 \pm 0.04$)

structure factor,

$$S(\vec{q}) = \frac{1}{N_{sites}} \sum_{\vec{i},\vec{j}} e^{-i\vec{q}(\vec{i}-\vec{j})} \langle (n_{\vec{i},\uparrow} - n_{\vec{i},\downarrow})(n_{\vec{j},\uparrow} - n_{\vec{j},\downarrow}) \rangle_0 \tag{33}$$

for an 8×8 lattice, $\rho = 50/64$, $U = 2$; $\rho = 42/64$, $U = 3$ and $\rho = 26/64$, $U = 3$. Although reduced in comparison to the half filled band, antiferromagnetic spin-spin correlations are still present between next neighbors. Long range correlations may still be seen especially at $\rho = 50/64$, $U = 2$ where there is a distinct antiferromagnetic correlation between the two furthest points on the lattice. The magnitude of this correlation is comparable to the half filled band case but is opposed in sign. At half filling, the magnetic structure factor shows a peak at $q = (\pi, \pi)$ which should diverge with increasing lattice sizes thus reflecting long range antiferromagnetic order. As the system is doped, the peak at $q = (\pi, \pi)$ splits into four peaks located at wave vectors $(\pi, \pi \pm \Delta q)$ and $(\pi \pm \Delta q, \pi)$. As the band filling is lowered, Δq grows and the magnitude of the peaks decreases. The form of the magnetic structure factor at off half band fillings is especially subject to finite size effects due to the incommensurate nature of the spin density wave. Unfortunately simulations on larger lattices and $\rho < 1$ were not realizable due to severe sign problems. The question about the divergence of the peaks in $S(q)$ with increasing lattice size remains open.

We have equally studied the occupation of single particle states through the quantity:

$$n(\epsilon) = \frac{\sum_{\vec{k},\sigma} \langle c_{\vec{k},\sigma}^{\dagger} c_{\vec{k},\sigma} \rangle_0 \delta(\epsilon - \epsilon(\vec{k}))}{\sum_{\vec{k},\sigma} \delta(\epsilon - \epsilon(\vec{k}))}. \tag{34}$$

Here, $\epsilon(\vec{k}) = -2t(\cos(k_x) + \cos(k_y))$ denotes the single particle eigenvalues of the kinetic energy in units of the lattice constant. Figure 12 plots $n(\epsilon)$ for $\rho = 1$ and $U = 2$, $U = 4$. At $\rho = 1$, the jump at the fermi level seems to disappear as appropriate for an insulator. For this filling, particle-hole charge-density fluctuations involve an energy gap set by U and an insulating state is expected. We have compared the Q.M.C. results to a mean field spin density wave approximation which predicts the opening of a gap Δ at the Fermi level. The magnitude of the gap is given by:

$$1 = \frac{U}{2N_{sites}} \sum_{\vec{k}} \frac{1}{(\epsilon^2(\vec{k}) + \Delta^2)^{\frac{1}{2}}} \tag{35}$$

For a 10×10 lattice and $U = 4$, equation (35) yields $\Delta/t = 1.38$. The mean field prediction of $n(\epsilon)$ is confronted to the Q.M.C. data in figure 12. Although meanfield yields a good qualitative fit to the Q.M.C. data, it overestimates the size of the gap. A *renormalized* gap of $\Delta_{Q.M.C.}/t = 1.07$ gives a better fit. For an
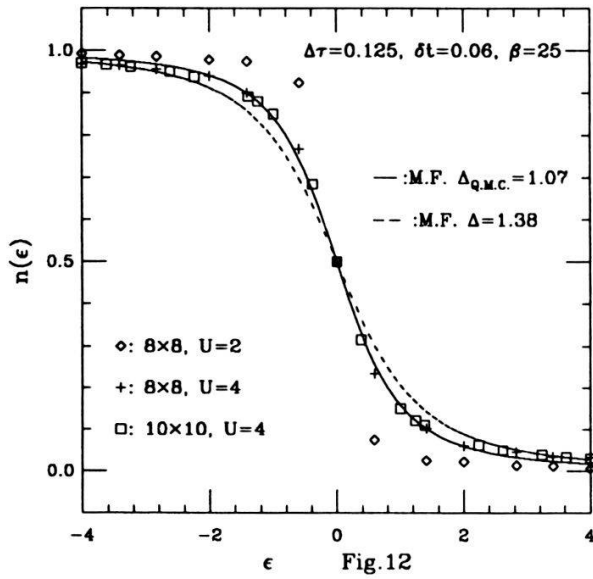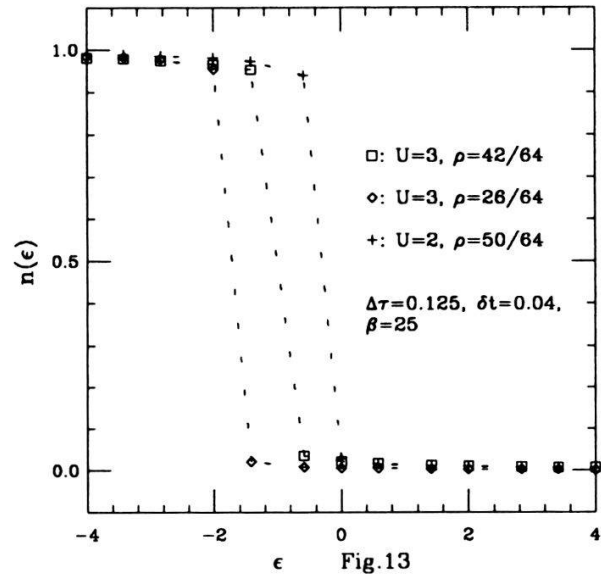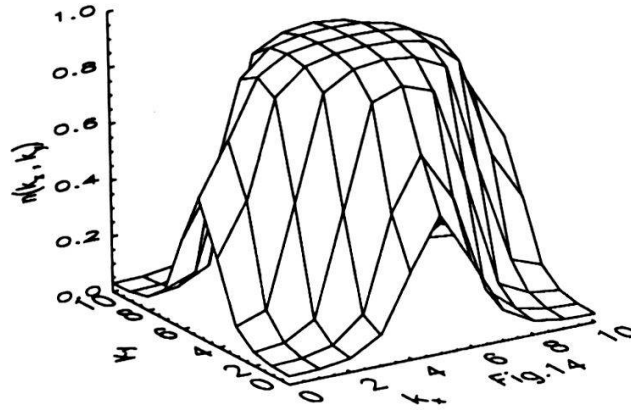
Fig.12 $n(\epsilon)$ for 8×8, 10×10 lattices at $\rho = 1$, $\beta = 25$, $U = 2$ and $U = 4$.

Fig.13 $n(\epsilon)$ for a 8×8 at $\rho = 50/64$ ($U = 2$), $\rho = 42/64$ ($U = 3$), $\rho = 26/64$ ($U = 3$) and $\beta = 25$.

Fig.14 $\langle c_{\vec{k}}^{\dagger} c_{\vec{k}} \rangle_0$ for a 10×10 lattice at $\rho = 1$, $U = 4$ and $\beta = 25$.

8×8 lattice at $U/t = 2$, equation (35) predicts $\Delta/t = 0.429$ whereas an optimal fit to the Q.M.C. data yields $\Delta_{Q.M.C.}/t = 0.378$. At off half band fillings, and small to moderate values of the on site Coulomb repulsion, meanfield predicts a paramagnetic ground state. Figure 13 plots $n(\epsilon)$ for an 8×8 lattice at various off half band fillings and values of U. The $U = 0$ sharp Fermi surface is much less smeared out by the on site Coulomb repulsion than at half band fillings. Again, for such fillings, the sign problem prevents us from carrying out simulations on larger lattices required to establish the existence of discontinuity at the Fermi level.

3   Conclusions

In comparison to the finite temperature algorithm [6], the ground state simulation method is expected to be more efficient at low fillings since the dimension of the matrices involved is of $N^{\uparrow,(\downarrow)} \times N^{\uparrow,(\downarrow)}$ rather than $N_{sites} \times N_{sites}$. The ground state algorithm is valid only if one is able to reach high inverse temperatures required to filter out the ground state from the trial wave function. This implies the capacity for dealing with numerical instabilities at low temperatures and with the sign problem. We have shown how to circumvent the problem of numerical instabilities at low temperatures. As for the average sign, our results show that it decays exponentially with growing inverse temperatures. However, for band fillings where the ground state of the non interacting system is not degenerate, high inverse temperatures may be reached without being confronted to a major sign problem. Unfortunately, simulations in the parameter range $0.8 < \rho < 1$ and $U > 2$ were not realizable due to severe sign problems. The ground state algorithm leaves the freedom of choosing the trial wave function. Depending on how clever one is at choosing it, the inverse temperature required to filter out the ground state may be significantly lowered. This is crucial in view of the sign problem. Very recently, Sorella et al. have proposed to use a Gutzwiller projected trial wave function and claim that inverse temperatures of $\beta \simeq 6/t$ are required to stabilize the ground state energy [22]. In summary, our Q.M.C. data supports the accepted picture of a Mott insulating antiferromagnetic ground state at half band filling. A mean field spin density wave approximation was found to overestimate the size of the gap at the Fermi level. When doped, the antiferromagnetic structure is drastically suppressed leaving place to an incommensurate spin density wave. Unfortunately, the sign problem prevents us from carrying out simulations on large lattices and off half band fillings. It remains the most challenging problem of Q.M.C. simulations of the Hubbard model.

Acknowledgements

References

[1] P.W. Anderson, Science 235 (1987) 1196

[2] F.C. Zhang and T.M. Rice, Phys. Rev. B 37 (1988) 3759

[3] D.Poilblanc, Phys. Rev. B 39 (1989) 140

[4] A. Parola, S. Sorella, M. Parrinello, and E. Tosatti, Preprint (1989).

[5] J. E. Hirsch, Phys. Rev. B 31 (1985) 4403

[6] S.R. White, D. J. Scalapino, R.L. Sugar, E.Y. Loh, J.E. Gubernatis,and R.T. Scalettar, Phys. Rev. B

[7] G. Sugiyama S. E. Koonin, Annals of Physics 168 (1986) 1.

[8] S. Sorella, E. Tosatti, S. Baroni, R. Car, and M. Parrinello Int. J. Mod. Phys. B 1 (1988) 993.
     S. Sorella, S. Baroni, R. Car, and M. Parrinello, Europhysics Letters 8 (1989) 663.

[9] M. Imada and Y. Hatasugai J. Phys. Soc. Jpn. 58 (1989) 3752.
     W. von der Linden, I. Morgenstern and H. de Raedt, IBM-Preprint (1989).

[10] F.F. Assaad, D. Würtz, submitted to Z. f. Phy. B.

[11] G.G. Batrouni, G. R. Katz, A. S. Kronfeld, G. P. Lepage, B. Svetitsky, and K. G. Wilson, Phys. Rev D 32 (1985) 2736.
     G. G. Batrouni, Phys. Rev D 33 (1986) 1815.

[12] G. Parisi and Wu Yongshi, Scientia Sinica 24 (1981) 483.

[13] A. D. Sokal, Cours de Trosième Cycle de la Physique en Suisse Romande Juin 1989 Lausanne.

[14] D. Tousaint, Arizona preprint AZPH-TH/89-6.

[15] F.F. Assaad and Ph. de Forcrand, IPS Research Report No. 89-07. To appear in Proceedings of Quantum Simulations of Condensed Matter Phenomena, Los Alamos (1989).

[16] J.E. Hirsch, R.L. Sugar, D. J. Scalapino, R. Blankenbecler, Phys. Rev. B 26 (1982) 5033

[17] S.R. White and J. W. Wilkins, Phys. Rev. B 37 (1988) 5024

[18] S.R. White, R.L. Sugar, R.T. Scalettar, Phys. Rev. B 38 (1988) 11665

[19] E. Y. Loh, J. E. Gubernatis, R.T. Scalletar, S.R. White, D. J. Scalapino, and R.L. Sugar, Preprint.

[20] A. Moreo, D.J. Scalapino, R.L. Sugar, S.R. White, N.E. Bickers, Preprint UCSBTH-89-28.

[21] We omit the extra sign which comes from the fact that we are not necessarily propagating the world lines between the same initial and final states.

[22] S. Sorella, PhD. Thesis.

[23] S. Sorella, A. Parola, M. Parrinello, and E. Tosatti, Preprint